(5) ten Brinke, G.; Karasz, F. K.; MacKnight, W. J. *Macromolecules* **1983**, *16*, 1827.
(6) Kambour, R. P.; Bendler, J. T.; Bopp, R. C. *Macromolecules* **1983**, *16*, 753.
(7) Paul, D. R.; Barlow, J. W. *Polymer* **1984**, *25*, 487.
(8) Izumitani, T.; Hashimoto, T. *J. Chem. Phys.* **1985**, *83*, 3694.
(9) Benmouna, M.; Benoit, H. *J. Polym. Sci., Polym. Phys. Ed.* **1983**, *21*, 1227.
(10) Boue, F.; Daoud, M.; Nierlich, M.; Williams, C., Cotton, J. P.; Farnoux, B.; Jannink, G.; Benoit, H.; Dupplessix, R.; Picot, C.; *Neutron Inelastic Scattering, Proc. Symp., 1977* **1978**, *1*, 563.
(11) LeGrand, A. D.; LeGrand, D. G. *Macromolecules* **1979**, *12*, 450.
(12) Hashimoto, T., unpublished paper.
(13) Mori, K.; Hasegawa, H.; Hashimoto, T., to be submitted to *Macromolecules*.
(14) Tanaka, H.; Hasegawa, H.; Hashimoto, T., to be submitted to *Macromolecules*.
(15) Hashimoto, T.; Mori, K.; Okawara, A.; Hasegawa, H., to be submitted to *Macromolecules*.
(16) Cahn, J. W.; Hilliard, J. E. *J. Chem. Phys.* **1958**, *29*, 258; **1959**, *31*, 688.
(17) This refers to the spinodal point for the order–disorder transition of block polymers (microphase separation) rather than that for the liquid–liquid phase separation between the two polymers.
(18) The enhanced miscibility is identical with the decreased order–disorder transition temperature of the block polymer systems.
(19) The χ_s values in Figure 13a were determined for the particular case of $N = 100$ (DP of A–(1/2)B). The χ_s values for other N's can be easily obtained by noting that $(\chi N)_s$ is invariant.
(20) When $f_1 = f_2$, there is no thermodynamic driving force that stabilizes the two-phase structure in the disordered state; i.e., the single phase is always the thermodynamically stable structure. Therefore one does not need to worry about the distinguishability. However, it is generally concluded that the distinguishability of the two systems becomes less as the offset of the f value becomes less.
(21) The relation $\chi_{eff} = \chi\phi_p$ is obtained from the mean-field approximation. As the concentration of polymer increases, the concentration-blob[3] size tends to decrease to the segmental size. In this limit polymer A and polymer B are mixed at the segmental level so that this relation between χ_{eff} and χ becomes exactly legitimate. Here we are not concerned with the accuracy of this relation, which determines the accuracy of χ estimated by this method. We are rather concerned whether or not the experimental profiles can be fitted with the theoretical profile by using the effective $\chi(\chi_{eff})$. The problems of polymer A + polymer B + neutral good solvent can be shown to have a one-to-one correspondence to the problems of polymer A + polymer B by replacing χ (for the systems without solvent) by the effective χ value.[23] Of course, the scaling prediction gives a relationship[22,23] between χ and χ_{eff} different from $\chi_{eff} = \chi\phi_p$.
(22) de Gennes, P.-G. *J. Polym. Sci., Polym. Phys. Ed.* **1978**, *16*, 1883.
(23) Onuki, A.; Hashimoto, T., in preparation.
(24) Leibler[2] defined N and R_g as polymerization index and radius of gyration of the entire block chain, respectively. In this case $q_m \simeq 2/R_g$ for $f = 1/2$. However, in Figure 1, N is defined as the polymerization index of A or B rather than that of the entire block polymer A–B in order to facilitate the comparison with the polymer mixture. Hence R_g in this figure corresponds to $R_g/2^{1/2}$ defined by Leibler. The rest of this paper follows Leibler's definition of N.
(25) IUPAC Commission on Macromolecular Nomenclature *Pure Appl. Chem.* **1985**, *57*, 1427.
(26) It should be noted that Olvera de la Cruz and Sanchez developed a new type of theory based on the path-integral approach.[27]
(27) Olvera de la Cruz, M.; Sanchez, I. *Macromolecules* **1986**, *19*, 2501.
(28) The numerical solutions were obtained down to the value $qR_{g1} = 0.03$ with good accuracy. The intensity $I(0)$ can be obtained in analytical form as in eq IV-5, from which the asymptotic behavior near $q = 0$ and its dependence on ϕ_1 are discussed.
(29) We assume block polymer ABR1–ABR2 can be prepared by a sequential polymerization of ABR1 block and ABR2 block.

Surface Light Scattering Study of a Poly(ethylene oxide)–Polystyrene Block Copolymer at the Air–Water and Heptane–Water Interfaces

Bryan B. Sauer and Hyuk Yu*

Department of Chemistry, University of Wisconsin, Madison, Wisconsin 53706

Chao-fong Tien† and Douglas F. Hager

Miami Valley Laboratories, Procter & Gamble Company, Cincinnati, Ohio 45247.
Received July 15, 1986

ABSTRACT: Spread films of a poly(ethylene oxide)–polystyrene diblock copolymer were studied at the air–water and heptane–water interfaces by using the Wilhelmy plate technique and surface quasi-elastic light scattering (SLS) from capillary waves. At the air–water interface, the dynamic film viscoelastic parameters, i.e., surface pressure, surface dilational elasticity and viscosity, and transverse viscosity, were deduced from the SLS measurements. The static surface tension and dilational elasticity were compared to their dynamic counterparts from SLS. At the heptane–water interface, the dynamic surface pressure and transverse viscosity were evaluated, and the latter was found to be zero for the whole surface concentration range. Some speculations about possible chain conformations of the copolymer at the two interfaces are offered.

Introduction

This is a study of a nonionic surfactant representative of an important and widely used group of nonionic surfactants containing ethylene oxide linkages as the hydrophilic component. We use here a low molecular weight sample ($M_n = 4135$) of a poly(ethylene oxide)–polystyrene block copolymer (PEO–PS). It can be spread on the air–water and heptane–water interfaces; hence the surface concentration is easily controlled (the air–water interface and heptane–water interface henceforth are referred to as A/W and O/W, respectively). A novel feature of the copolymer is the hydrophobic component, i.e., PS segments,

†Present address: Science Center, Air Products and Chemicals, Inc., Allentown, PA 18105.

0024-9297/87/2220-0393$01.50/0

which have no polar side chains. This is contrasted to a poly(vinylpyrrolidone)–poly(vinyl acetate) copolymer previously studied,[1] which has polar side chains in both segments.

The technique of surface light scattering (SLS) from capillary waves is a powerful new tool for studying spread films because one gains access to film viscoelastic parameters. SLS has been used to study polymer[2,3] and small-molecule films[2,4-7] at A/W. Interpretations of the results, however, are still under active discussion. By focusing on contrasting behaviors of a given system at both interfaces, we hope to gain insight into the dynamic character of spread films. To our best knowledge we are the first to study spread films at O/W using SLS,[8] and in this paper we give a more detailed analysis of the capabilities of the technique at O/W.

Theoretical Background

Film viscoelastic parameters have been extracted from SLS results previously at A/W,[2-7] but these measurements suffer, as do ours, by virtue of having too many unknown parameters. Under certain conditions, however, simplifying assumptions can be made so as to reduce the number of unknown parameters.[2] The dispersion relation[9,10] describes the capillary wave motions at A/W and is used to extract film viscoelastic properties from the SLS data. It is represented as

$$[\eta(k + m) - \epsilon^* k^2/i\omega][\eta m(k + m)/k - \sigma^* k^2/i\omega] = \eta^2(k - m)^2 \quad (1)$$

where η = shear viscosity of bulk water, $k = (2\pi/\lambda) \sin \phi \cos \theta$, λ = laser wavelength, ϕ = scattering angle, θ = incident angle measured from normal to surface, $m = [k^2 - i\omega\rho/\eta]^{1/2}$, $\omega = 2\pi f_s - 2\pi i(\Delta f_{s,c}/2)$, f_s = frequency shift (or peak frequency), $\Delta f_{s,c}$ = corrected frequency full width at half-height, ρ = density of water, $\epsilon^* = \epsilon - i\omega\kappa$, ϵ = surface dilational elasticity, κ = surface dilational viscosity, $\sigma^* = \sigma - i\omega\mu$, σ = surface tension, and μ = surface transverse viscosity. The difference between the left-hand side and the right-hand side of eq 1 is set equal to zero to solve the equation for the parameters of interest. For simple liquids without any surface films, this equation is simplified because $\epsilon^* = 0$ and $\mu = 0$. For film-covered surfaces, the situation becomes more complicated because longitudinal waves on the surface couple with the transverse capillary waves. Although the longitudinal waves makes a negligible contribution to the light scattering intensity, they can affect the actual motion of the transverse capillary waves.[2] The longitudinal dilational waves are controlled by the film parameters ϵ and κ, both of which have shear components[11] that cannot be separated from the dilational components by SLS. A frequency-dependent term in σ^* has been defined as the surface transverse viscosity μ. Goodrich[12] has earlier provided a simple physical picture of μ.

To give an idea of the dependence of the two experimental quantities f_s and $\Delta f_{s,c}$ on the viscoelastic parameters, Hård and Löfgren[4] have calculated f_s and $\Delta f_{s,c}$ as functions of ϵ and κ. According to their calculations, f_s is weakly dependent on ϵ whereas $\Delta f_{s,c}$ is quite sensitive. For example, $\Delta f_{s,c}$ increases by almost 200% from the pure liquid value at an intermediate value of 0.2 for the reduced elasticity ϵ/σ, the ratio of the dilational elasticity to the surface tension. The dependence of f_s and $\Delta f_{s,c}$ on the other film viscoelastic parameter, μ, has also been calculated by Langevin.[2]

A light scattering study has been performed recently with spread films of a phospholipid at O/W in one of our laboratories.[8] It was found that the light scattering spectra were completely different from those obtained at A/W relative to the damping behavior whereas the film elastic properties were rather comparable at both interfaces. Lucassen-Reynders and Lucassen[13] have also seen a large difference between the induced capillary wave motion for adsorbed films at A/W and O/W. The dispersion relation at O/W[14] is given below using the notation of Löfgren et al.[15]

$$[\eta_w(k + m_w) + \eta_d(k + m_d) - \epsilon^* k^2/i\omega] \times [\eta_w m_w(k + m_w)/k + \eta_d m_d(k + m_d)/k - \sigma^* k^2/i\omega] = [\eta_w(k - m_w) - \eta_d(k - m_d)]^2 \quad (2)$$

where subscript w refers to water, subscript d refers to the oil phase, and the other variables are as defined after eq 1. Solving eq 2 with the input parameters of η_w, η_d, ρ_w, ρ_d, k, and σ, one obtains the dependence of f_s and $\Delta f_{s,c}$ on ϵ at different values of κ and μ. A particular set with k = 459 cm^{-1} and σ = 50.83 dyn/cm for the heptane–water interface is shown in Figures 1 and 2, where the independent variable is expressed as the reduced dilational elasticity ϵ/σ. Because the densities and viscosities of the two phases are comparable at O/W, there exists negligible coupling between longitudinal dilational waves and transverse capillary waves. This is clearly illustrated in Figure 1. In the most sensitive case, i.e., $\kappa = 0$, $\Delta f_{s,c}$ increases only by about 8% as the coupling becomes progressively more

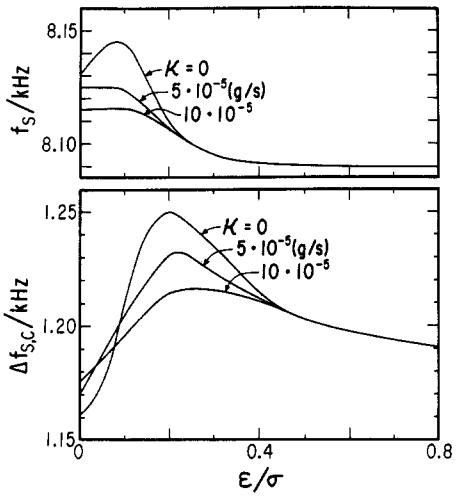

Figure 1. Theoretical predictions of frequency shift f_s and frequency width $\Delta f_{s,c}$ as a function of the reduced surface dilational elasticity ϵ/σ at different dilational viscosities κ at a scattering wave vector of k = 459 cm^{-1} and interfacial tension of σ = 50.83 dyn/cm at O/W.

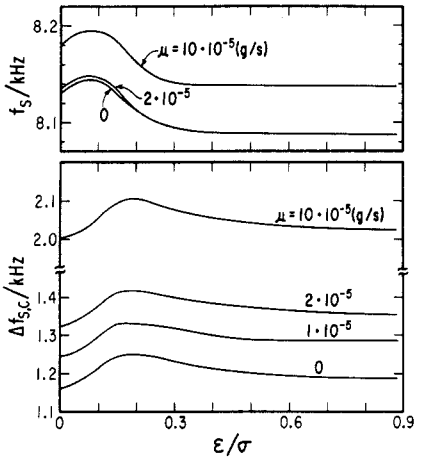

Figure 2. f_s and $\Delta f_{s,c}$ vs. ϵ/σ at different transverse surface viscosities μ at O/W. The same values for k and σ as in Figure 1 were used.

Table I
Calibration Summary at 25 °C

order	k/cm^{-1}	f_s/Hz	Δf_{obsd}/Hz	Δu_i/mm	Δf_i/Hz	$\Delta f_{s,c}$/Hz	σ_{int}/(dyn/cm)	η/cP
				Air–Water				
4	262	5689	630	0.72	401	374	71.3	0.95
5	323	7821	754	0.635	393	549	72.0	0.92
6	385	10176	1015	0.76	514	755	72.0	0.89
7	445	12597	1200	0.72	523	972	71.6	0.86
							71.97[a]	0.890[a]
				Heptane–Water				
5	335.8	5110	740	0.61	235	665		
6	400.0	6625	950	0.48	201	907	(50.8)	(0.39)
7	460.7	8168	1240	0.67	301	1167		
8	522.7	9856	1540	0.69	300	1470		
							50.8[b]	0.39[c]

[a] Reference 20. [b] Reference 21. [c] Reference 22.

efficient from the bare interface ($\epsilon/\sigma = 0$) to the maximal extent when the reduced elasticity reaches a value of 0.2. The corresponding change on A/W[4] comes to almost 200%. Furthermore, Figure 1 also shows that the magnitude of variation in $\Delta f_{s,c}$ becomes smaller as κ is increased. The magnitude of variation in f_s, however, amounts to only a trivial change for all cases, which is not very different from that at A/W.

Analogous plots at different values of the transverse viscosity are given in Figure 2. It is evident that the transverse viscosity, if present, could have a large effect on the light scattering spectra, which is rather similar to the predicted effect at A/W.[2]

Experimental Section

Materials. The block copolymer was synthesized in two steps by an anionic procedure. The synthesis was carried out in a standard high-pressure apparatus according to the procedure of O'Malley and Marchessault.[16] After the apparatus was dried and evacuated to 10^{-6} Torr, it was sealed. A cumylpotassium solution (5 mL, 0.9 M) as the initiator in tetrahydrofuran (THF) was added to the reaction flask via a breakseal. The initiator, cumylpotassium, was prepared by reacting the dipotassium salt of the tetramer of α-methylstyrene with cumyl methyl ether. Stirring was started and 3.8 g (0.0365 mol) of purified styrene in 40 mL of THF was added to the reactor at 0 °C. The molecular weight of the resulting polystyrene was about 2400. The reactor was then cooled to −78 °C. Purified ethylene oxide (1.2 g, 0.027 mol) was added to the reactor, and the contents were shaken for a few minutes. The contents were then transferred to a thick-wall reaction tube and allowed to warm to ambient temperature. After the red color of the polystyrylpotassium disappeared, the tube was heated to 70 °C for 3 days. The polymer solution was then neutralized with acetic acid, and the polymer was isolated by precipitation with heptane.

The mean mole ratio of styrene to ethylene oxide in the copolymer was determined by proton NMR. Weight- and number-average molecular weights were determined by gel permeation chromatography. The number-average molecular weight was confirmed by vapor phase osmometry. These techniques characterized the sample synthesized above as having the mole ratio of 1.33 PEO/PS and an overall M_n of 4135 with the molecular weight distribution approximately indicated by $M_w/M_n = 1.19$. Thus, the sample has on the average 34 and 25 monomeric units respectively of PEO and PS.

The heptane (Aldrich, 99%) was purified with 60–100-mesh Florisil magnesium silicate and then doubly distilled. The water used here was house distilled water further purified with a Milli-Q filtering system (Millipore) with one carbon and two ion-exchange filters. Dichloromethane (Aldrich, spectrophotometric grade, Gold Label) was used without further purification as the spreading solvent.

Methods. Air-Water Interface. Both SLS and static measurements were performed in a Langmuir trough milled out of Teflon having the dimensions of 28.5 cm × 11.1 cm × 1.0 cm, enclosed in a Plexiglas box (68 cm × 30 cm × 24 cm) with the relative humidity kept at 70%. A 1.0 cm × 2.5 cm sandblasted platinum plate attached to a Cahn 2000 electrobalance was used as the Wilhelmy plate for determining the static surface pressure. The film was compressed by moving a Teflon barrier at A/W. The surface temperature was controlled to ±0.1 °C at 25 °C by circulating thermostated water through a glass coil placed at the bottom of the trough. By performing the SLS simultaneously with the static measurements, it was possible to make a direct comparison between the two techniques.

The light scattering instrument was designed after Hård and Nilsson,[17], and its detailed description has appeared elsewhere.[18] The essential feature of the instrument is the use of a transmission grating to provide local oscillator sources for heterodyne beating at the cathode surface of the photomultiplier and to afford us with a ready means to select a well-defined scattering angle for each diffraction order of the grating. The grating is illuminated with a 7-mW He/Ne laser (Melles Griot), and a combination of two lenses is used to focus simultaneously the real image of the grating on the scattering surface and the diffraction spots on the photocathode. The scattering angle was defined by the diffraction order and the optical configuration. The spatial separation of the diffraction spots was measured by translating a 20-μm pinhole across the diffraction spots to pinpoint the intensity maximum positions, allowing the scattering angle to be calculated. The full width at half-height of the Gaussian intensity distribution of each spot was found by means of the same moving pinhole, and the spatial width is simply referred to as the instrumental profile (Δu_i). The heterodyne power spectrum, acquired on the spectrum analyzer (Nicolet 444A), was subsequently analyzed by fitting to Lorentzian profile. The replicability of the peak shift f_s and the observed full width at half-height Δf_{obsd} were about 0.5% and 5%, respectively. Provided that the instrumental profile is Gaussian and that the corrected width ($\Delta f_{s,c}$) is larger than one-half of Δf_{obsd}, eq 3 is used to correct for the instrumental width according to the procedure of Hård et al.[19]

$$\Delta f_{s,c} = \Delta f_{obsd} - \Delta f_i^2/\Delta f_{obsd} \quad (3)$$

where the instrumental width Δf_i is calculated by using the instrumental profile as in eq 4

$$\Delta f_i = 2^{3/2}\pi(df_s/dk)(\cos\theta/R\lambda)\Delta u_i \quad (4)$$

Here, df_s/dk is the experimentally determined derivative of frequency shift with respect to k, where k is the scattering wave vector. The incident angle measured normal to the interface is θ (64.4°), R is the distance from the interface to the photomultiplier (356.0 cm), λ is the laser wavelength (632.8 nm), and the instrumental profiles (Δu_i) at each diffraction order, i = 4, 5, 6, and 7, are collected in Table I along with the corresponding k values. Since df_s/dk is different at each surface concentration, Δf_i must be calculated for each concentration according to eq 4.

Heptane–Water Interface. The SLS experiments for O/W were performed with the same instrument as that on A/W. The only modifications were the use of a 4-cm BK-7 equilateral glass prism (Melles Griot) to guide the horizontally polarized laser light past the air–heptane interace and also the use of another deeper Teflon trough (10.8 cm × 10.8 cm × 1.7 cm). Its temperature was controlled to ±0.1 °C at 25 °C by water circulation through the

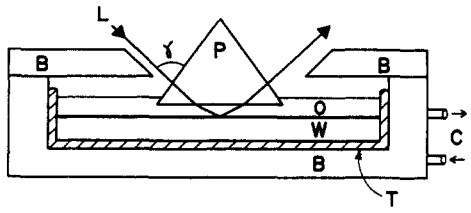

Figure 3. Schematic of the light-guiding prism orientation with respect to the heptane–water interface. Here, L is the laser beam with incident angle normal to the prism ($\gamma = 94.4°$), the incident angle measured normal to the O/W interface is 76°, P is the prism, O is the oil phase (4 mm deep), W is the aqueous phase (8 mm deep), B is the brass casing, T is a 3-mm-thick Teflon shell, and C is the inlet/outlet for water circulation. The prism holder and brass cover are not shown.

brass casing. The scattering cell assembly is schematically shown in Figure 3, where the prism holder and base plate are not shown for clarity. All other optics are the same as previously reported.[18]

Two different methods were used to spread the sample on the heptane–water interface. The first was to layer successively small amounts (μL) of a dichloromethane solution of the sample onto the interface. We call this the continuous addition method. Blank experiments with just dichloromethane were performed to confirm that solvent alone has no effect on the interfacial tension. The second method was to spread first the sample onto A/W and subsequently layer heptane onto the water phase. We designate this as the single-shot method because for each surface concentration, the entire procedure must be repeated. The two methods gave the same results for the range of surface concentration $0 < \Gamma < 50 \times 10^{-5}$ mg/cm^2. Beyond $\Gamma = 50 \times 10^{-5}$ mg/cm^2, the film was no longer stable and homogeneous; this was confirmed by the observation of flakes of the sample when sweeping O/W after spreading with the single-shot method. Note that no static measurements were performed simultaneously with the SLS measurements on O/W. This came about because of the use of the new scattering cell with the light-guiding prism where the size of the prism in contact with the oil phase constrained the thickness of the oil phase to 4 mm at the maximum, which precluded complete immersion of the Wilhelmy plate for the static measurements.

Similarly to the case of A/W, the scattering angle and instrumental width correction must be determined at O/W. Because of optical distortion due to the prism and heptane vapor, we resorted to back-calculating the scattering angle and instrumental profile using a calibration standard, the heptane–water interface. The procedure was examined in detail by validating a set of scattering angles and instrumental profiles, which were then used to calculate correctly the interfacial tensions and viscosities of several simple organic liquids layered on the water subphase. The procedure has been reported in a recent publication[8] from one of our laboratories.

The following is the procedure for the back-calculation with the heptane–water interface as the calibration standard. First, f_s and Δf_{obsd} (in place of $\Delta f_{s,c}$, which is yet to be determined) at a given diffraction order are substituted into the dispersion relation, eq 2, along with the literature values for the viscosities and densities of water[20] and heptane and for the interfacial tension of heptane–water,[21] and a first trial k is then estimated. Next, we choose a value for $\Delta f_{s,c}$ near Δf_{obsd} and combine this with the first trial k to deduce a viscosity of heptane. Then, $\Delta f_{s,c}$ is varied until the literature value for the viscosity of heptane[22] is obtained. This now gives us a first set of k and $\Delta f_{s,c}$. The small difference between Δf_{obsd} and $\Delta f_{s,c}$ causes k to deviate slightly, so the process is iterated once more. First, k is varied until the correct value for the interfacial tension is obtained, and then $\Delta f_{s,c}$ is readjusted until the literature value for the viscosity of the heptane phase is obtained. For each diffraction order, we repeat the procedure.

The final step is to calculate the instrumental width Δf_i from both $\Delta f_{s,c}$ and Δf_{obsd} using eq 3. From Δf_i, Δu_i is calculated by using eq 4, and this is listed in Table I for $i = 5$, 6, 7, and 8 along with the respective k values. Once the instrumental profile Δu_i is calculated, it is used as a constant for all polymer concentrations. For each concentration, however, Δf_i must be calculated by using Δu_i and the observed df_s/dk.

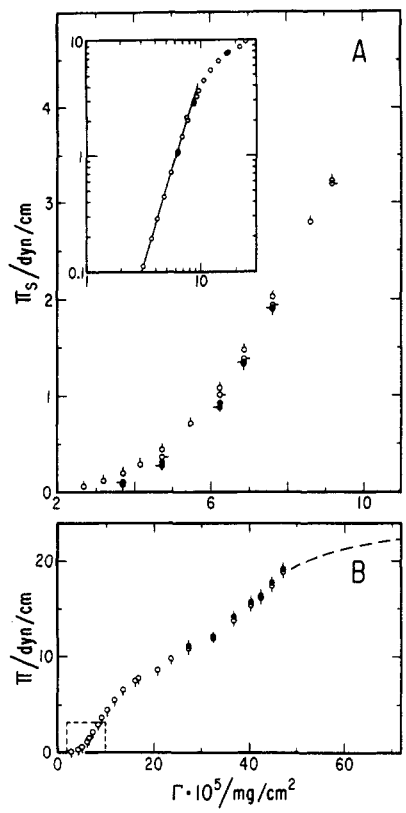

Figure 4. (A) Static surface pressure Π_s vs. surface concentration Γ for the PEO–PS copolymer in the dilute region at A/W. The two full cycles of compression and expansion are represented by first compression (◇), first expansion (◆), second compression (○), and second expansion (●). The inset is a log–log plot for the first compression showing a power law region below $\Pi_s = 2.5$ dyn/cm. (B) Plot of static (○) and dynamic surface pressure (●) vs. Γ for the entire concentration range. The dashed square in the lower left corner is the region plotted in (A) and the dashed curve in the upper right corner indicates the region of reversibility failure (see text for details).

Results and Discussion

A/W. We first present the results of studies conducted at A/W. At the outset we ascertained that the sample forms a stable spread film by performing a reversibility experiment. This is shown in Figure 4A, where the static measurement results are presented for the less concentrated surface region, $\Gamma = (2\text{–}10) \times 10^{-5}$ mg/cm^2. By effecting two full cycles of compression and expansion, we found a slight hysteresis on the expansion branch. Upon compression, however, the surface pressure regained the original value. We take this as evidence that neither irreversible multilayer formation nor desorption of the spread film into water has occurred. In the inset of the figure, we plot the data on a log–log scale and find a slope of 3.38 ± 0.02. This is to be contrasted to the scaling law prediction[23] of 2.85 for linear homopolymers in two dimensions under semidilute good solvent conditions and the experimental verification of 2.85 for PEO homopolymers.[24] Although we do not as yet understand its significance, it appears certain that there exists a power law regime of Π_s relative to Γ at least for about one-half logarithmic decade in Γ. For the moment, it seems sufficient to note that our sample is not a linear homopolymer but a block copolymer with hydrophilic and hydrophobic components as in other surfactant molecules.

Figure 4B gives a pressure–concentration curve for the entire concentration range, and the dashed line square in the lower left corner indicates the region plotted in Figure 4A. The segment of dashed curve in the upper right corner

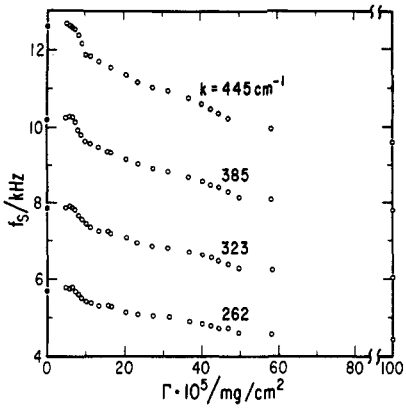

Figure 5. Frequency shift vs. Γ at four different scattering wave vectors k at A/W. The filled circles on the ordinate axis are the data for bare water surface.

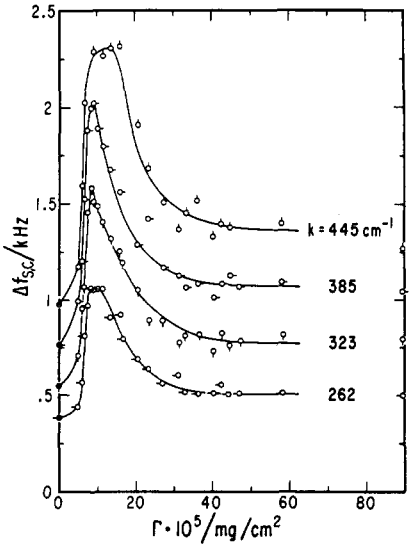

Figure 6. Corrected frequency width vs. Γ at four different scattering wave vectors k at A/W. The smooth curves are drawn over the data points to indicate the trend, and the filled circles are for zero surface concentration, i.e., bare water surface.

represents a region where reversibility did not occur. Upon compression of the film past 50×10^{-5} mg/cm^2 followed by expansion, there was a substantial (5–6 dyn/cm) hysteresis, indicating perhaps irreversible multilayer formation or desorption. At any rate, we have now defined the range of Γ beyond which the data are no longer reproducible. In addition to the static measurement data indicated by open circles with pips, we have included in the figure the dynamic measurement data by filled circles. Agreement between the two sets is rather gratifying. We will fully discuss these dynamic data later.

We now turn to the SLS results at A/W. In Figures 5 and 6 are shown f_s and $\Delta f_{s,c}$, respectively, as a function of Γ at different k values. In both figures, filled circles without and with pips on the ordinate axes are those obtained on a bare water surface, i.e., Γ = 0. It is noteworthy that f_s does not decay correspondingly with Γ from the bare water value in our four cases. Instead, there exists a region, (0–5) $\times 10^{-5}$ mg/cm^2, wherein f_s remains practically the same or possibly increases slightly before an abrupt decrease sets in. Others have observed a similar trend[2,3] with poly(vinyl acetate) at A/W, and this is to be expected according to theoretical predictions.[2] From the observed reversibility of Π_s up to $\Gamma = 50 \times 10^{-5}$ mg/cm^2 there can be no solubility of the sample into the water subphase. This trend is to be contrasted to $\Delta f_{s,c}$ shown in Figure 6

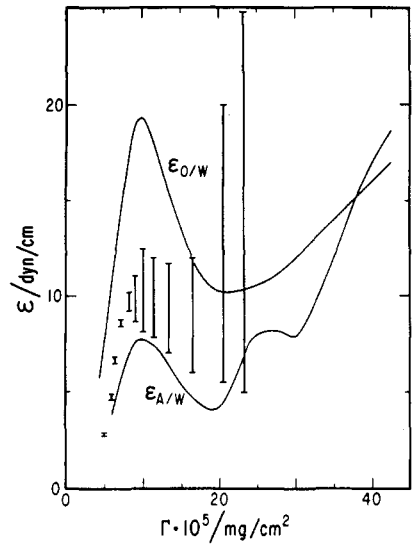

Figure 7. Static elasticity (lower curve), dynamic elasticity (vertical bars) at A/W, and static elasticity at O/W are plotted against Γ. The upper and lower bounds of the vertical bars are detailed in the text.

where it peaks at $\Gamma = 10 \times 10^{-5}$ mg/cm^2 for all four k vectors. The curves in the figure are drawn smoothly over the data. As the representative theoretical calculations of Langevin[2] show, the peak corresponds to the maximum coupling of the longitudinal and capillary waves. This would mean that the temporal damping of the capillary waves maximizes when the most efficient resonance condition exists between the two kinds of surface waves, though capillary waves alone should contribute to the light scattering. An additional contrast of the two is afforded by noting that the peak position in Figure 6 corresponds approximately to the end of the initial abrupt decrease of f_s in Figure 5. Without further evidence it is difficult to pinpoint exactly what the molecular conformation of our sample is like at this point. Nevertheless, we propose that the peak position for this sample corresponds to the onset of a uniform monolayer state. A rough estimate at $\Gamma = 10 \times 10^{-5}$ mg/cm^2 is obtained for a uniform film thickness of 10 Å if the film density is taken to be 1 g/cm^3.

While the copolymer conformations at various stages are yet to be delineated and it would surely take substantial efforts to do so, we can proceed with the phenomenological characterization of the films via their viscoelastic parameters using f_s and $\Delta f_{s,c}$. We effect the calculations under two different sets of assumptions. The nature of the assumptions depends on the magnitude of ϵ in the region of interest. In the more dilute region from 0 to 25×10^{-5} mg/cm^2 where the elasticity is intermediate, ϵ and κ are calculated under the following set of assumptions: (1) dynamic surface pressure (Π) $\geq$ static surface pressure (Π_s), (2) $\kappa \geq 0$, and (3) $\mu = 0$. The dynamic elasticity ϵ thus calculated can be compared to the static elasticity ϵ_s, which is calculated from the concentration dependence of Π_s according to

$$\epsilon_s = \Gamma(d\Pi_s/d\Gamma) \tag{5}$$

In Figure 7, we show ϵ_s and ϵ at A/W. The lower curve designated as $\epsilon_{A/W}$ represents the ϵ_s values calculated from the data of Figure 4 according to eq 5, and the vertical bars are its dynamic counterparts ϵ calculated from the dispersion relation, eq 1, with the above-stated assumptions. The curve designated as $\epsilon_{O/W}$ is deferred to later. The determination of ϵ is quite precise between 5×10^{-5} and 8×10^{-5} mg/cm^2 while between 8×10^{-5} and 20×10^{-5} mg/cm^2 the range of imprecision in the determination of

ϵ is rather large. Those arising from the fourth-order diffraction (k = 262 cm^{-1}) were ignored for these calculations because they gave inconsistent results. This was due to the instrumental width being comparable to the corrected width, therefore making eq 3 no longer applicable for the instrumental correction (see Table I). We emphasize that these ranges for ϵ are not uncertainties in measurements but are simply imprecisions in the data analysis due to the assumptions stated above. In other words, we calculate a finite range for ϵ because there are three unknowns and only two experimental parameters, $\Delta f_{s,c}$ and f_s.

The upper limits of ϵ correspond to $\Pi = \Pi_s$, and as Π is allowed to become greater than Π_s in the calculation, ϵ tends to decrease. Note that $\Pi \equiv \sigma(0) - \sigma(\Gamma)$, where $\sigma(0)$ is the surface tension of bare water. This latter term is the same for both static and dynamic measurements.[18] Around 20 × 10^{-5} mg/cm^2, ϵ starts to become quite large, making the light scattering insensitive to ϵ. Hence above 23 × 10^{-5} mg/cm^2, ϵ can no longer be calculated; for example, at Γ = 31.3 × 10^{-5} mg/cm^2, incrementing $\Pi = \Pi_s$ to $\Pi = \Pi_s$ + 0.1 (dyn/cm) changes ϵ from 0 to 50 dyn/cm, making it impossible to compute a reliable value. Thus a comparison of ϵ and ϵ_s is only meaningful up to Γ = 20 × 10^{-5} mg/cm^2. The general trend of the two is in good accord, but their magnitudes do differ slightly; ϵ and ϵ_s both maximize at Γ = 10 × 10^{-5} mg/cm^2, the same point of Γ as the peak position of $\Delta f_{s,c}$ in Figure 6. Beyond this, a favorable comparison may also be made about the dip position at Γ = 20 × 10^{-5} mg/cm^2, corresponding to an inflection point of the Π_s–Γ plot in Figure 4B. We will offer later a speculation as to what might be happening to the copolymer molecules at this point. For the moment, however, our focus is placed on the general trend of ϵ and ϵ_s relative to their Γ dependences. For Γ > 20 × 10^{-5} mg/cm^2 at A/W, the static data appear to reveal another small bump and dip at 25 × 10^{-5} and 30 × 10^{-5} mg/cm^2, respectively. However, the precision of taking the first-order derivative of Π_s with respect to Γ was such as to obscure any significance in the observation. There should, however, be another well-defined maximum in $\epsilon_{A/W}$ around Γ = (40–50) × 10^{-5} mg/cm^2, as is obvious from the Figure 4B. On the other hand, we have stopped $\epsilon_{A/W}$ at Γ = 40 × 10^{-5} mg/cm^2 in Figure 7 since the static measurements were not reversible beyond about 50 × 10^{-5} mg/cm^2 as mentioned earlier.

Using the same set of assumptions in the dilute region, we calculated κ values at different Γ values, and these are collected in Table II. Since the trend is fairly monotonic, we did not plot them separately. Furthermore the lower bound is always zero; hence only the upper bound values, corresponding to the assumption that $\Pi = \Pi_s$, are summarized in the table. The κ values are quite similar in magnitude to the others previously estimated from SLS results[2,6,7] but are much larger than κ for the PEO homopolymer,[25] which never exceeds 3 × 10^{-5} surface poise for the frequency range. Note that surface poise has the cgs unit of g/s. As seen from the last column of Table II, the dilational viscosity amounts to no more than 10% of the elasticity up to Γ = 10 × 10^{-5} mg/cm^2 but precipitously increases to 86% by the time Γ reaches 20 × 10^{-5} mg/cm^2. This is the region of Γ where we speculate that PEO segments protrude into the water phase.

We now concern ourselves with film properties in the high-concentration region. As alluded to earlier in conjunction with the discussion of Figures 1 and 2, the SLS power spectra are quite insensitive to ϵ and κ at A/W as these reach beyond certain threshold values. This brings us naturally to invoke the second set of assumptions for a range of Γ above 25 × 10^{-5} mg/cm^2. Following the method of Langevin,[2] Π and μ can be calculated by setting ϵ and κ equal to some reasonably large values. The Π values calculated in this manner have an uncertainty of ±0.3 dyn/cm, mostly due to the assumptions made relative to ϵ and κ. These are shown in Figure 4B along with the static value, Π_s. There are no dynamic surface pressures shown below Γ = 25 × 10^{-5} mg/cm^2 in the figure.

Table II
Surface Concentration Γ, Upper Bounds of Surface Dilational Viscosity κ, and the Relative Contribution of the Viscosity to the Elasticity, $2\pi f_s\kappa/\epsilon_{max}$,[a] at A/W (the Lower Bound Is Always Zero)

Γ × 10^5, mg/cm^2	κ × 10^5,[b] g/s	$2\pi f_s\kappa/\epsilon_{max}$
5.0	0 ± 0.3	0
5.9	0.7 ± 0.5	0.10
6.5	1.5 ± 0.5	0.14
7.2	1.0 ± 0.5	0.07
8.2	1.6 ± 0.5	0.1
9.0	2.7 ± 0.3	0.15
10.1	4.4 ± 0.5	0.21
11.5	6.0 ± 0.4	0.30
13.4	8.5 ± 0.5	0.43
16.5	12 ± 2	0.59
20.6	30 ± 10	0.86
23.4	50 ± 40	0.81
27.2	90 ± 10	[c]
31.3	140 ± 50	[c]

[a] f_s used here is for k = 385 cm^{-1}, and ϵ_{max} is the corresponding upper bound value in Figure 7 for A/W. [b] Surface poise has the unit of g/s. [c] Indeterminate.

In the same concentrated region μ was also explicitly calculated and was found to be zero with an experimental error of ±5 × 10^{-6} g/s (surface poise). This seems reasonable since this is not the first time that values of μ have been found to be zero at the high surface pressures, including polymer films[2] at A/W. It should be noted that Langevin[2] is one of the few to have found the need to invoke μ to fit experimental data. She estimated that μ was finite only for a small region in the vicinity of the maximum $\Delta f_{s,c}$. Using one of the same samples as Langevin,[2] Hård and Neuman[6] found no need to rely on μ to fit their data. From our experience, the determination of Π, ϵ, κ, and μ from the two experimental parameters f_s and $\Delta f_{s,c}$ in this region of maximum $\Delta f_{s,c}$ (Figure 6) does give rise to uncertainties in the exact values of any one of these parameters. Crilly and Earnshaw have found a finite μ for condensed monolayers of glycerol monooleate at A/W[26] and suspended bilayers of the same compound in water.[27,28] For the suspended bilayers the calculation of μ is easily made since the transverse modes are completely independent of the longitudinal modes because the viscosity and density of the water above and below the bilayer are the same. All this evidence taken together indicates that the detection of μ seems to depend on the sample studied. Taking advantage of the fact that the static film elasticities are similar for A/W and O/W whereas the capillary wave damping properties are drastically different, we can calculate μ unambiguously over the whole concentration range at O/W as will be discussed presently.

O/W. As stated in the beginning of this paper, we refer to the heptane–water interface as O/W. Similar to A/W, the power spectra from O/W are fit to a Lorentzian profile yielding f_s and Δf_{obsd}. From the results displayed in Figures 8 and 9, it is apparent that rather different behavior from that seen at A/W occurs. The first point to be contrasted is the Γ dependence of f_s in Figure 8. Unlike that at A/W (Figure 5), f_s at O/W has a very small range of invariance with Γ, if at all; essentially, f_s decays immediately and

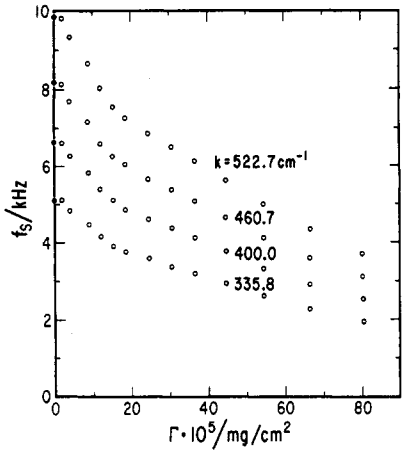

Figure 8. Frequency shift vs. Γ at O/W at four different k values. The filled circles are zero surface concentration.

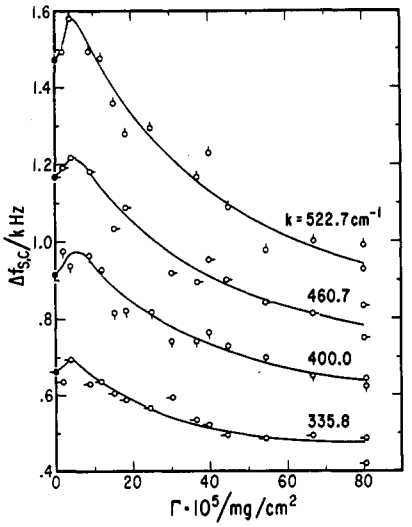

Figure 9. Corrected frequency width vs. Γ at O/W at four different k values. The smooth curves are drawn over the data points to indicate the trend, and the filled circles are for zero surface concentration.

monotonically with Γ, and the range of variation is much larger than that at A/W, indicating that our copolymer is exceedingly surface active at O/W. There, also, is no region of abrupt decrease with Γ while such was observed at A/W. The second point of contrast has to do with only a slight hint of the coupling between the longitudinal and capillary waves. This is shown in Figure 9, where $\Delta f_{s,c}$ has a small maximum around $\Gamma = 5 \times 10^{-5}$ mg/cm^2. In particular, the magnitude of the maximum at $k = 460.7$ cm^{-1} (second from the top) amounts to about 80 Hz, which is very close to that predicted in Figure 1 when $\kappa = 0$ at $\epsilon/\sigma = 0.2$. The third point of contrast is at the high-concentration end around 80×10^{-5} mg/cm^2, where $\Delta f_{s,c}$ has not as yet reached any asymptotic limit at O/W, while at A/W $\Delta f_{s,c}$ reached the asymptote at around $\Gamma = 40 \times 10^{-5}$ mg/cm^2. Fourthly, ϵ and κ have a very small effect on the SLS spectra over most of the surface concentration range as mentioned above. Thus, the dispersion relation, eq 2, can be solved directly for $\sigma(\Gamma)$, and hence for Π. In Figure 10, we plot the Π values so obtained against surface area per PEO monomer unit, A, which is a variable inversely proportional to Γ by

$$A = 201/(\Gamma \times 10^5) \quad (\text{Å}^2/\text{PEO monomer}) \quad (6)$$

where Γ is expressed in units of mg/cm^2. The choice of A as the independent variable in the figure will shortly

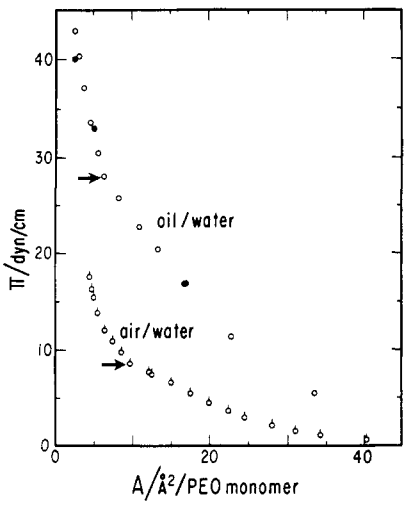

Figure 10. Surface pressure vs. area per PEO monomer (A). The lower curve (○) represents A/W and the upper curve represents O/W. For O/W, the solid circles represent the single-shot spreading method and the open circles represent the continuous addition method. The arrows indicate discontinuities in the slope (see text for details).

become apparent. The data points by the continuous addition method (open circles) and the single-shot method (filled circles) apear to be identical up to 50×10^{-5} mg/cm^2 or $A = 4$ Å^2/PEO monomer in Figure 10. At $A = 4$ Å^2/PEO monomer there is a 4 dyn/cm discrepancy, which can be explained by incomplete spreading. As mentioned in the Methods section, when the copolymer was spread at 4 Å^2/PEO monomer using the single-shot method, large flakes of copolymer could be seen.

The transverse surface viscosity μ was calculated simultaneously with Π. It was found to be zero within experimental error of $\pm 5 \times 10^{-6}$ g/s over the whole concentration range. We have also found μ to be zero for monolayers of phospholipid,[8] PEO homopolymer,[25] and poly(vinyl acetate)[25] at the heptane–water interface. Crilly and Earnshaw[27,28] are the only others to perform SLS on films at liquid–liquid interfaces. They found transverse viscosities on the order of 5×10^{-5} g/s for glycerol monooleate bilayers.[28] It is evident that more systems must be studied before we truly understand μ.

We have shown on another occasion that Π calculated from SLS measurements and Π_s obtained from static measurements are the same at O/W over a large interfacial pressure range,[8,25] so that we need not treat the two sets, Π and Π_s (or ϵ and ϵ_s), differently. We can therefore use Π and Π_s interchangeably at O/W. The result is the upper curve of Figure 7, where ϵ_s is identified as $\epsilon_{O/W}$. First, turning to the significance of $\epsilon_{O/W}$ vis-à-vis $\epsilon_{A/W}$ in Figure 7, the film dilational elasticity of our sample at O/W is greater than that at A/W by about a factor of 2 up to $\Gamma = 20 \times 10^{-5}$ mg/cm^2, beyond which the difference appears to diminish. We do not show the behavior beyond $\Gamma = 40 \times 10^{-5}$ mg/cm^2 since film stability becomes suspect at this point. In a separate study,[25] we have also shown that the elasticity profiles of PEO homopolymer relative to the surface concentration of PEO segments are in substantial agreement with those in Figure 7; $\epsilon_{A/W}$(homopolymer) $\simeq$ $\epsilon_{A/W}$(copolymer), and $\epsilon_{O/W}$(homopolymer) $\simeq$ $\epsilon_{O/W}$(copolymer) for $0 \leq \Gamma \leq 15 \times 10^{-5}$ mg/cm^2. Hence, the difference in magnitude of $\epsilon_{A/W}$ and $\epsilon_{O/W}$ appears to arise solely from the PEO segments. We do not understand, however, at the moment how such a difference comes about, either in the homopolymer or in the copolymer. We therefore take this as an indication that the area per molecule is predominantly determined by the PEO seg-

ment for $\Gamma < 15 \times 10^{-5}$ mg/cm^2 and that this is true at both interfaces. This is the reason that we have chosen A as the independent variable in Figure 10. On the other hand, the effect of the PS segments in the sample seems to be revealed at $\Gamma > 20 \times 10^{-5}$ mg/cm^2, in the surface pressure region where the PEO homopolymer no longer exhibits any film properties; i.e., film collapse has taken place. Coming to the peak position of ϵ at $\Gamma = 10 \times 10^{-5}$ mg/cm^2 for all four instances, A/W and O/W for the copolymer and the PEO homopolymer (not shown here), we tentatively propose that this is derived from the uniform monolayer state of PEO segments and that beyond this point they start to protrude into the water phase. Even though the capillary waves are insensitive to ϵ at O/W, the elasticity data in Figure 7 can be used to predict where the maximum in $\Delta f_{s,c}$ should occur in Figure 9. Using the theoretical predictions in Figure 1, we expect this maximum to occur when $\epsilon/\sigma = 0.2 = 10/50$. With respect to $\epsilon_{O/W}$, at $\Gamma = 6 \times 10^{-5}$ mg/cm^2 it has a value of 10 dyn/cm, and this is the concentration where $\Delta f_{s,c}$ maximizes in Figure 9.

We now offer our speculations with regard to the molecular conformations at A/W and O/W. From Figure 10 it is evident that there are "kink points" (discontinuities in slopes indicated by arrows for clarity) at 8 and 27 dyn/cm at A/W and O/W, respectively. Recent results with the PEO homopolymer have shown that the collapse pressures are 6.5–7.5 dyn/cm at A/W[24] and 21 dyn/cm at O/W.[25] Since the kink points for the copolymer occur near the collapse pressures of the homopolymer at both interfaces, we attribute the kink points to the maximum possible protrusion (chain dangling) of the PEO segments into the water phase. An ancillary piece of evidence is derived from the observation of a large increase in the ratio $2\pi f_s k/\epsilon_{max}$ at A/W (the last column of Table II), which may be regarded as the relative increase in the dilational viscosity due to PS segments as PEO segments protrude into the water phase. We can go further and note that at pressures above the kink points each copolymer molecule still occupies a substantial area, indicating that the PS segments are actually occupying a large interfacial area at A/W and O/W. A similar observation has been made previously by Labbauf and Zack[29] with polystyrene–poly(methyl methacrylate) diblock copolymers.

Summary

Using a combination of SLS and static Wilhelmy plate measurements at air–water and oil–water interfaces, we have studied spread films of a PS–PEO diblock copolymer. The copolymer served as an ideal system to make a comparison of SLS at A/W and O/W, allowing several conclusions to be drawn. At O/W, the longitudinal modes do not couple efficiently with the transverse modes of the surface waves; thus ϵ and κ have almost no influence on the capillary wave motions making precise determinations of the dynamic surface pressure Π and transverse surface viscosity μ. The latter was found to be zero for the entire concentration range for O/W. At A/W, on the other hand, a strong coupling of longitudinal and capillary waves allowed the determination of both ϵ and κ at low concentrations assuming $\mu = 0$. The dynamic elasticity exhibited a similiar trend as its static counterpart. At high concentrations, the coupling is lost because ϵ is large, so the Π and μ could be determined. The value of μ was found to be zero once again.

Another comparison at A/W was made between Π_s determined by the plate method and Π from SLS. Excellent agreement was observed in the higher concentration regions at A/W. This should quell any fears that the contact angle is perturbed by this film using the Wilhelmy method at A/W.

Acknowledgment. This work was in part supported by the Research Committee of the University of Wisconsin—Madison, the University Exploratory Research Program of Procter & Gamble Co., and Kodak Research Laboratories. We are most grateful to our colleagues at Wisconsin, George Zografi, Yen-Lane Chen, Kyung-Hwa Yoo, and Hyungsuk Pak, for fruitful discussions.

References and Notes

(1) Zatz, J. L.; Knowles, B. *J. Pharm. Sci.* **1971**, *60*, 1731.
(2) Langevin, D. *J. Colloid Interface Sci.* **1981**, *80*, 412.
(3) Kawaguchi, M.; Sano, M.; Chen, Y.-L.; Zografi, G.; Yu, H. *Macromolecules* **1986**, *19*, 2606.
(4) Hård, S.; Löfgren, H. *J. Colloid Interface Sci.* **1977**, *60*, 529.
(5) Byrne, D.; Earnshaw, J. C. *J. Phys. D: Appl. Phys.* **1979**, *12*, 1133.
(6) Hård, S.; Neuman, R. D. *J. Colloid Interface Sci.* **1981**, *83*, 315.
(7) Chen, Y. L.; Sano, M.; Kawaguchi, M.; Yu, H.; Zografi, G. *Langmuir* **1986**, *2*, 349.
(8) Sauer, B. B.; Chen, Y.-L.; Zografi, G.; Yu, H. *Langmuir* **1986**, *2*, 683.
(9) Bouchiat, M. A.; Meunier, J. *J. Phys. (Paris)* **1971**, *32*, 561.
(10) Langevin, D.; Bouchiat, M. A. *C. R. Seances Acad. Sci., Ser. B* **1971**, *272*, 1422.
(11) Mann, J. A. *Langmuir* **1985**, *1*, 10.
(12) Goodrich, F. C. *J. Phys. Chem.* **1962**, *66*, 1858.
(13) Lucassen-Reynders, E. H.; Lucassen, J. *Adv. Colloid Interface Sci.* **1969**, *2*, 347.
(14) Kramer, L. *J. Chem. Phys.* **1971**, *55*, 2097.
(15) Löfgren, H.; Neuman, R. D.; Scriven, L. E.; Davis, H. J. *J. Colloid Interface Sci.* **1984**, *98*, 175.
(16) O'Malley, J. J.; Marchessault, R. H. *Macromol. Synth.* **1972**, *4*, 35.
(17) Hård, S.; Nilsson, O. *Appl. Opt.* **1979**, *18*, 3018.
(18) Sano, M.; Kawaguchi, M.; Chen, Y.-L.; Skarlupka, R. J.; Chang, T.; Zografi, G.; Yu, H. *Rev. Sci. Instrum.* **1986**, *57*, 1158.
(19) Hård, S.; Hamnerius, Y.; Nilsson, O. *J. Appl. Phys.* **1976**, *47*, 2433.
(20) In *CRC Handbook of Physics and Chemistry*, 56th ed.; Weast, R. C., Ed.; CRC: Cleveland, OH, 1975.
(21) Aveyard, R.; Haydon, D. A. *Trans. Faraday Soc.* **1965**, *61*, 2255.
(22) Fleischer, D. In *Polymer Handbook*; Brandrup, J., Immergut, E. H., Eds.; Wiley: New York, 1975.
(23) Le Guillou, J. C.; Zinn-Justin, J. *Phys. Rev. Lett* **1977**, *39*, 95.
(24) Kawaguchi, M.; Komatsu, S.; Matsuzumi, M.; Takahashi, A. *J. Colloid Interface Sci.* **1984**, *102*, 356.
(25) Sauer, B. B.; Kawaguchi, M.; Yu, H., to be published.
(26) Crilly, J. F.; Earnshaw, J. C. In *Biomedical Applications of Laser-Light Scattering*; Sattelle, D. B., Lee, W. I., Ware, B. R., Eds.; Elsevier/North-Holland: Amsterdam, 1982; p 123.
(27) Crilly, J. F.; Earnshaw, J. C. *Biophys. J.* **1983**, *41*, 197.
(28) Crilly, J. F.; Earnshaw, J. C. *Biophys. J.* **1983**, *41*, 211.
(29) Labbauf, A.; Zack, J. R. *J. Colloid Interface Sci.* **1971**, *35*, 569.